

# Electrical and thermal control of Fabry-Pérot cavities mediated by Casimir forces

Lixin Ge,<sup>1,\*</sup> Bingzhong Li,<sup>1</sup> Hao Luo,<sup>1</sup> and Ke Gong<sup>1</sup>

<sup>1</sup>*School of Physics and Electronic Engineering, Xinyang Normal University, Xinyang 464000, China*

(Dated: October 13, 2023)

Dynamic tuning of optical cavities is highly desired in many photonic systems. Here, we show that Fabry-Pérot (FP) cavities can be actively controlled by the Casimir force. The optical FP cavities consist of a gold nanoplate confronted to an electrical-connecting multi-layer substrate in a liquid environment. The gold nanoplate can be stably suspended due to the balance of repulsive and attractive Casimir forces. Moreover, the suspension distance are modulated strongly by the electric gating or temperature of the system. As a result, we could shift the resonant wavelengthes of the cavities with tens of nanometers at optical frequencies. Finally, we analyze the influence of Brownian motion on the equilibrium distances. Due to the high  $Q$ -factor of the FP cavities, our proposed system offers a remarkable platform to experimentally investigate the thermal Casimir effect at sub-micrometer separations

PACS numbers:

## I. INTRODUCTION

The Casimir force between two perfect metallic plates, predicted by Hendrik Casimir in 1948, is a macroscopic quantum effect resulting from the zero-point fluctuations in vacuum [1]. Latter, this quantum effect was generalized by E. M. Lifshitz to include frequency-dependent dielectrics and finite temperatures [2]. The Casimir forces between two objects consisted by the same materials are generally attractive. In the past two decades, great effort has been devoted to the search for Casimir repulsions in the vacuum environment[3–10], yet lack of experimental verifications due to the strict constrains. By contrast, the Casimir repulsions have been experimentally achieved between two liquid-separated objects (labelled 1 and 2) when the permittivity satisfies  $\varepsilon_1(i\xi) > \varepsilon_{\text{liq}}(i\xi) > \varepsilon_2(i\xi)$  for a vast range of frequency [11], where  $\varepsilon_{\text{liq}}(i\xi)$  is the permittivity of the intervening liquid evaluated with imaginary frequency  $\omega = i\xi$ . Interestingly, stable suspensions mediated by Casimir repulsions were reported in different configurations[12–17].

Recently, an new concept for tunable FP cavities has been proposed by Estes et al.[18], based on the Casimir force. The FP cavities play a crucial role in optical spectroscopy and find extensive applications[19]. For instance, the FP cavities consisted of metal-insulator-metal have been received considerable interest in nanophotonics, due to their excellent performances on strong light-matter interactions [20–22]. In general, the resonances of FP cavities are fixed once the samples are fabricated [18]. The dynamic tuning of optical FP cavities through the Casimir force, particularly using external stimuli such as electric gating, and temperature, remains largely unknown in this field.

Tunable Casimir forces can be realized by changing the dielectric response of the materials through exter-

nal stimuli, e.g., electric gating [23, 24], magnetic fields [25–27], optical lasers [28, 29], etc. Another scheme to dynamically tune the Casimir forces is based on the change of temperature [30–33]. Generally, thermal effect on the Casimir forces is weak [34, 35]. For a vacuum gap, the thermal Casimir effect is observable only when the separation is large (e.g., over three micrometers)[35]. Such large separation severely affects its applications. Recently, a strong thermal Casimir effect based on graphene sheets was revealed at sub-micrometer scales [36–39]. The temperature dependence of Casimir forces for graphene is attributed to two different mechanisms. The first one is the thermal fluctuation, as illustrated by the implicit term in [40]. The second one relies on the fact that the dielectric response of graphene is temperature dependence (the explicit term in [40]). This kind of temperature modulation can be manifest at shorter separations.

In this study, we aim to dynamically tune FP cavities by manipulating the Casimir forces. Our system comprises a gold nanoplate and a Teflon-coated metal-oxide-semiconductor (MOS) substrate. Notably, the Casimir forces acting on the suspended gold nanoplate exhibit a strong dependence on both the gating voltage and the temperature. As a result, the equilibrium separation of the gold nanoplate undergoes significant alterations. The resonant wavelength of the optical FP cavities can be shifted for tens of nanometers. These remarkable shifts can be accurately detected using state-of-the-art experimental techniques. At the end, the Brownian motion of nanoplates is taken into account, and our study presents an accurate approach for measuring thermal Casimir forces at sub-micrometer separations via spectroscopic of the cavities.

## II. THEORETICAL MODELS

Figure 1(a) illustrates the schematic of the system under study. In this setup, a gold nanoplate is suspended in

\*Electronic address: [lixinge@hotmail.com](mailto:lixinge@hotmail.com)

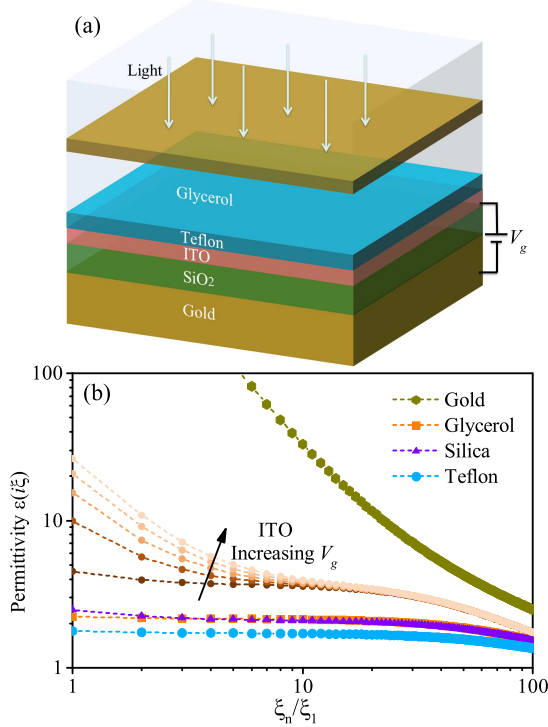


FIG. 1: (color online) (a) Schematic view of the system. The incident light is a plane wave, and the two parallel reflecting mirrors are consisted of the gold nanoplate and the gold substrate. (b) The dielectric response of materials evaluated in imaginary frequency. The plot depicts the permittivity of the accumulation layer of ITO, where the gating voltage increases from 0 to  $V_b$  with a step size of  $V_b/4$ .

a liquid of glycerol. The materials of Teflon, indium tin oxide (ITO), silica, and glycerol, are almost transparency at optical frequencies. Hence, the two parallel reflecting mirrors of the optical FP cavities are the suspended gold nanoplate and the gold substrate. There exists an electrical connection between the gold substrate and the ITO layer, which can be controlled by a gating voltage.

Considering the in-plane dimension of nanoplate is much larger than the separation, a proximity force approximation is applied for the calculations. The Casimir force is calculated by  $F_c = -\partial E_c(d)/\partial d$ , where  $E_c(d)$  is the Casimir energy between the nanoplate and the multilayer substrate:[12]

$$\frac{E_c(d)}{A} = k_B T \sum_{n=0}^{\infty} \int \frac{d^2 \mathbf{k}_{\parallel}}{(2\pi)^2} \log \det [1 - \mathbf{R}_1 \cdot \mathbf{R}_2 e^{-2K_n d}], \quad (1)$$

where  $A$  represents the in-plane area,  $k_B$  is the Boltzmann's constant,  $T$  is the temperature,  $d$  is the separation, the prime denotes a pre-factor 1/2 for  $n=0$ ,  $\mathbf{k}_{\parallel}$  is the parallel wavevector,  $K_n = \sqrt{k_{\parallel}^2 + \varepsilon_{liq}(i\xi_n)\xi_n^2/c^2}$  is the vertical wavevector in the liquid,  $\xi_n = 2\pi \frac{k_B T}{\hbar} n$  ( $n = 0, 1, 2, 3 \dots$ ) is the discrete Matsubara frequencies,  $\hbar$  is the reduced Planck's constant,  $c$  is the speed of light in

vacuum.  $\mathbf{R}_{1,2}$  is the  $2 \times 2$  reflection matrix, given by

$$\mathbf{R}_j = \begin{pmatrix} r_j^s & 0 \\ 0 & r_j^p \end{pmatrix}, \quad (2)$$

where  $r_j^\alpha$  with  $j=1$  and  $j=2$  are the reflection coefficients for the upper and lower layered structures, and the superscripts  $\alpha = s$  and  $p$  correspond to the polarization of transverse electric (TE) and transverse magnetic (TM) modes, respectively. The reflection coefficients are associated with the layer thicknesses and permittivity of materials, which can be calculated by a transfer matrix method (TMM)[41].

The generalized Drude-Lorentz model is applied for the gold[41]. The dielectric models and parameters for the materials of Teflon, silica, and glycerol are adopted from the recent literatures [42, 43]. The permittivity for the ITO film is evaluated by the Kramers-Kronig relationship:

$$\varepsilon(i\xi_n) = 1 + \frac{2}{\pi} \int_0^{\infty} \frac{\text{Im}[\varepsilon(x)]x}{x^2 + \xi_n^2} dx. \quad (3)$$

The absorption of the ITO materials (imaginary part) is constructive by the sum of the Drude model [44] and the Tauc-Lorentz model [45, 46]. Under electrical-bias, the ITO layer is divided into two distinct regions: the background layer and the accumulation layer. The carrier densities in these two layers are represented as  $N_b$  and  $N_a$ , respectively. The magnitude of  $N_b$  is fixed upon fabrication, whereas the magnitude of  $N_a$  can be adjusted by varying the gating voltage. As given in previous literatures, the accumulation layer possesses a homogeneous carrier density, and its thickness is determined by[24, 47]:

$$L_a = \frac{\pi}{\sqrt{2}} \sqrt{\frac{k_B T \varepsilon_0 \varepsilon_{ITO}}{N_b e^2}}, \quad (4)$$

where  $e$  is the electron charge,  $\varepsilon_0$  is the vacuum permittivity,  $\varepsilon_{ITO}=9.3$  is the static permittivity of ITO. In this work, The thickness of the ITO layer is fixed to be 5 nm, and the background carrier density  $N_b = 10^{19} \text{ cm}^{-3}$ . We have  $L_a = 2.56 \text{ nm}$  at  $T=300 \text{ K}$ . On the other hand, the analytical expression of  $N_a$  is given by [24]:

$$N_a = N_b + \frac{\varepsilon_0 \varepsilon_s V_g}{e L_s L_a}, \quad (5)$$

where  $\varepsilon_s=3.9$  denotes the static dielectric constant of silica,  $V_g$  is the applied voltage, and it should be smaller than the breaking down voltage  $V_b = E_b L_s$ , where we assume the breakdown field  $E_b = 30 \text{ MV/cm}$  [48, 49].

The permittivity evaluated in the imaginary frequency is presented in Fig. 1(b). Notably, the dielectric functions of the ITO in the accumulation layer exhibit significant variations with increasing voltages in the infrared frequency range. Teflon possesses the lowest permittivity, making it particularly desirable for Casimir repulsions at small separations. Although the permittivity of glycerol is close to that of silica at infrared and visible frequencies, its static permittivity, about 42.4, at zero frequency is much larger than that of silica.

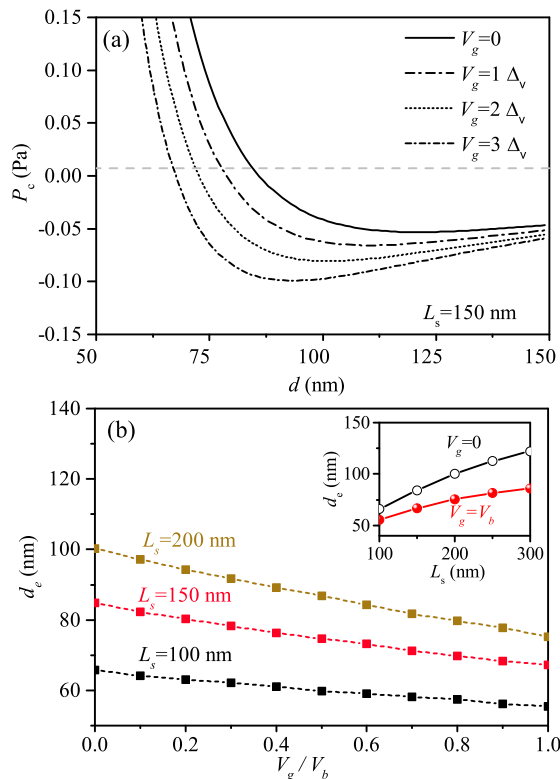


FIG. 2: (color online) (a) The Casimir pressures under different gating voltages, where  $\Delta_v = V_b/3$ , where the breakdown voltage is 450 V. The positive (negative) sign of the pressure corresponds to the repulsive (attractive) force. The gray dashed line represents the pressure generated from the gravity and buoyancy. (b) The equilibrium distances as a function of applied voltages. The inset shows the equilibrium distances as a function of the thickness of silica layer.

### III. RESULTS AND DISCUSSIONS

The Casimir pressure of suspended gold nanoplate versus the separation is shown in Fig. 2(a). The thickness of the gold nanoplate, Teflon, ITO, and silica layers are set to be 40, 10, 5, and 150 nm, respectively. The results demonstrate a significant modulation of the Casimir pressure by the gating voltage. At small separations, the Casimir pressure is repulsive, while it turns to be an attractive force for larger separations. A separation for zero pressure, known as the Casimir equilibrium, is identified at a specific separation. With increasing the voltages, the pressure tends to be attractive, and the separation for the Casimir equilibrium decreases correspondingly. In the absence of voltage, the Casimir equilibrium appears at approximately 85 nm, which decreases by about 18 nm as the voltage approaches to  $V_b$ . For a gold nanoplate with thickness of 40 nm, the pressure resulting from gravity and buoyancy is estimated to be 0.007 Pa [41], and is represented by the dashed grey lines in Fig. 2(a). The equilibrium distance, denoted as  $d_e$ , is established through the delicate balance among the Casimir force,

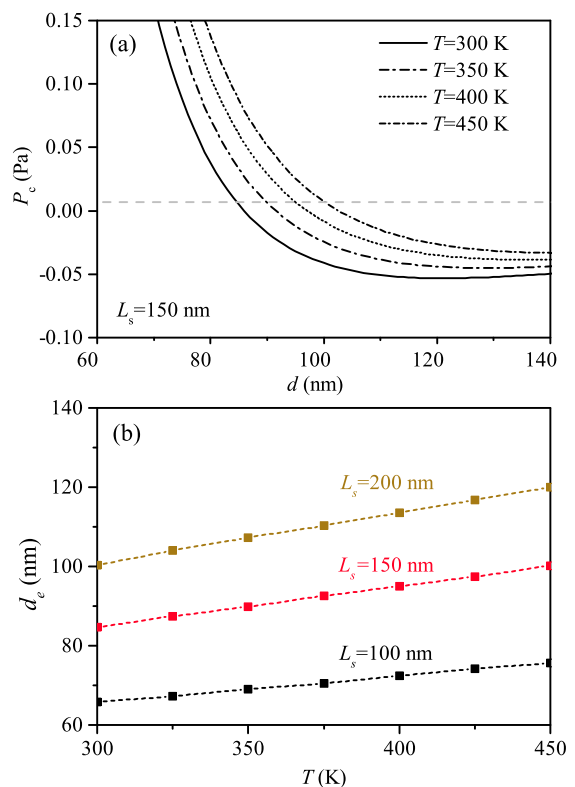


FIG. 3: (color online) (a) The Casimir pressures for different temperatures, where there is no applied voltage. The gray dashed line represents the pressure generated from the gravity and buoyancy. (b) The equilibrium distances as a function of temperature.

gravity, and buoyancy. The  $d_e$  is slightly smaller than the separation of Casimir equilibrium.

The equilibrium distance as a function of applied voltage is depicted in Fig. 2(b). The findings demonstrate a decline in the equilibrium distance as the voltage increases, ranging from 0 up to  $V_b$ . The equilibrium distance is also influenced by the thickness of the silica layer, as shown for  $L_s = 100, 150$  and 200 nm. The inset of Fig. 2(b) reveals that increasing the layer thickness, would result in elevated equilibrium distances, and the difference of  $d_e$  between  $V_g = 0$  and  $V_g = V_b$  expands. At  $L_s = 300$  nm, the difference of  $d_e$  for the  $V_g = 0$  and  $V_g = V_b$  reaches nearly 36 nm. The calculations suggest that the equilibrium distance, so as the resonant length, of the FP cavities can be effectively modulated by the tunable Casimir forces through electrical gating.

The Casimir pressure is also strongly dependent on the temperature, as shown in Fig. 3(a). The layer thicknesses of the materials are kept the same as those in Fig. 2(a). To manifest the temperature effect on the Casimir force, the applied voltage is assumed to be zero. We find that the Casimir pressure tends to be more repulsive as the temperature increases, and the variation of  $d_e$  is near 10 nm when the temperature increases from 300 to 400 K. The Casimir pressure as a function of temperature is

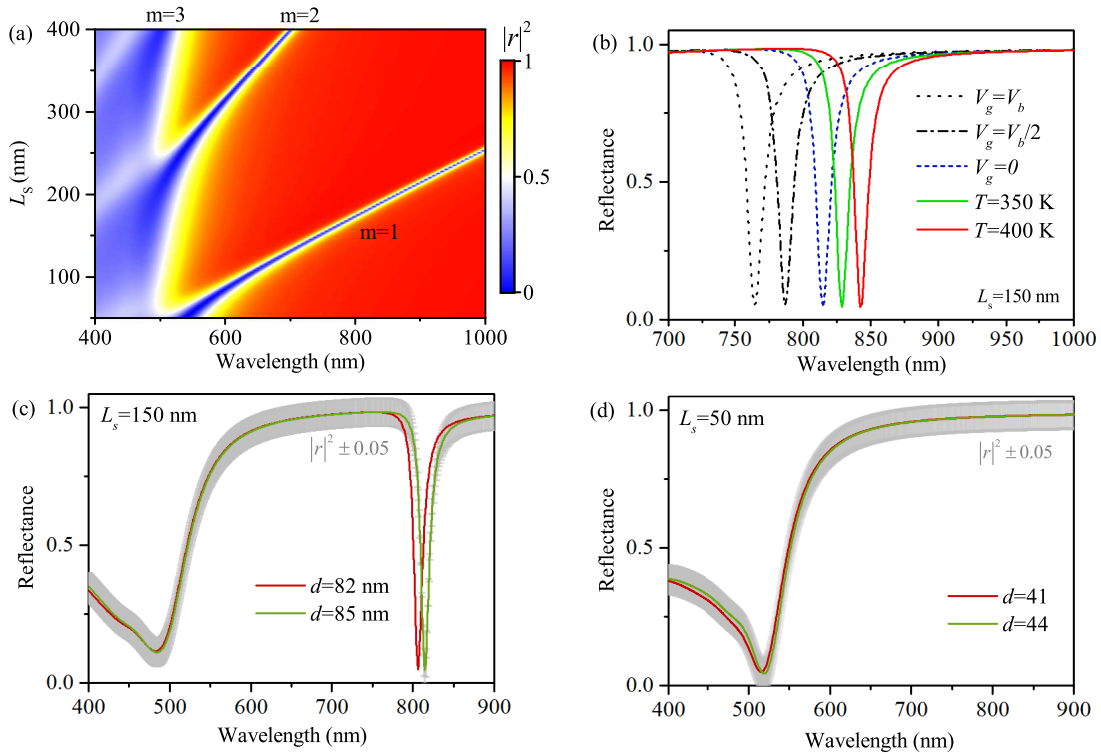


FIG. 4: (color online) (a) The reflectance of FP cavity varies with the layer thickness of silica, where the separation  $d$  is fixed at 60 nm. (b) The modulation of reflectance through the applied voltage and temperatures. (c) and (d) show the reflection spectra in and out of the equilibria. The equilibrium distances for  $L_s=150$  nm and  $L_s=50$  nm are 85 nm and 44 nm, respectively. The assumed error of the reflectance with  $\pm 0.05$  is given for the equilibrium separation represented by the gray bars.

shown in Fig. 3(b) under different  $L_s$ . Again, the value of  $d_e$  increases when the layer thickness  $L_s$  increases from 100 to 200 nm. The variation of  $d_e$  with respect to  $T$  is almost linear as reported in [50]. Such effective modulation of  $d_e$  due to the temperature has been proposed for detection of thermal Casimir effect [51]. However, the optical resonances have not been employed in the literature [50, 51].

The thickness of silica needs to be carefully designed. The contour plot of the reflectance via silica thickness and wavelength  $\lambda$  is shown in Fig. 4(a), wherein the separation  $d$  is fixed at 60 nm. The reflectance is calculated by the TMM in the real frequency [52]. The results reveal that different resonant modes are excited when the thickness  $L_s$  varies from 50 to 400 nm. A fundamental mode with  $m=1$  is excited in the visible regime when the layer thickness  $L_s$  is in proper range. As the thickness increases to a higher value, e.g., 300 nm, other high-order modes are presented.

Figure 4(b) show the reflection spectra under different external stimuli, where the nanoplate is suspended at the equilibrium distance  $d_e$ . The resonance of the FP cavities is modulated efficiently by the applied voltage and temperature. The equilibrium distances are about 85, 75 and 67 nm for the applied voltage are 0,  $V_b/2$  and  $V_b$ , respectively. On the other hand, the equilibrium distances increase to 90 and 95 nm for the temperatures 350 and

400 K, respectively. Hence, the resonant dip has a blue shift for increasing the voltages, while it has a red shift for increasing the temperature. The results show that the giant shifting of the resonances over tens of nanometers, is achieved by electrical gating or temperatures.

In a real configuration, the imperfection of the experiments (e.g., misalignment, surface roughness, electrostatic forces...) may exist, and the errors of the reflectance with  $\pm 0.05$  (gray lines) should be introduced as indicated in [18]. Here, the high  $Q$ -factor of optical cavities provides an avenue for accurate spectroscopic measurements. For instance, the resonant wavelength without the electrical gating appears at about 810 nm, where the equilibrium separation is 85 nm. When the separation is out of equilibrium with  $d=82$  nm, the resonant wavelength can be clarify by the spectroscopy, as shown in Fig. 4(c). The calculated results indicate that such small errors have limited influences as long as the spectra having high  $Q$ -factors. For thickness  $L_s=50$  nm, the equilibrium separation is 44 nm, and the shift of the reflection spectrum could not clarify in Fig. 4(d). This is because the resonance of the cavities appear at the lossy regime ( $\lambda$  is smaller than about 550 nm) with  $L_s=50$  nm, the change of reflection spectrum due to the the variation of separation could not be detected by the spectroscopy at such configuration.

The Brownian motion should be considered when the

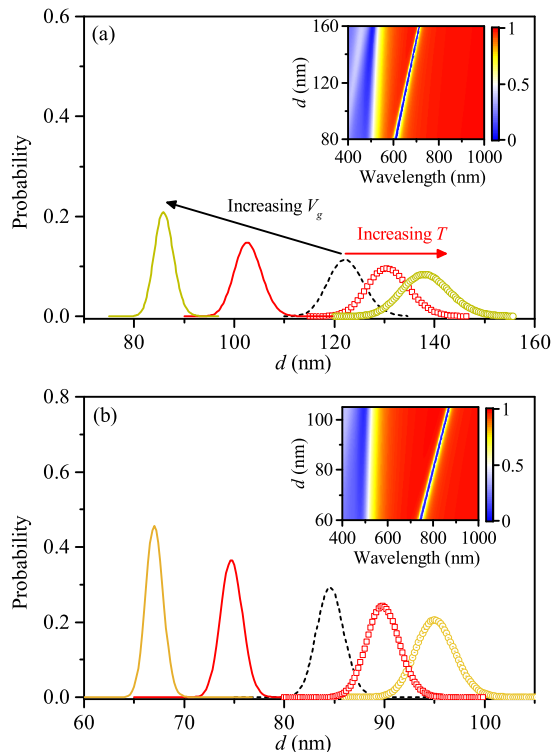


FIG. 5: (color online) The probability of suspension positions due to the Brownian effect with (a)  $L_s=300$  nm and (b)  $L_s=150$  nm. The increasing voltages are 0,  $V_b/2$ , and  $V_b$ . The increasing temperatures are 300, 350 and 400 K. The dashed lines represent the initial state with  $V_g=0$  and  $T=300$  K. The insets in (a) and (b) show the corresponding contour maps of the reflectance.

suspended nanoplate is finite size. The random Brownian motion happens at both lateral and vertical directions. The lateral Brownian motion does not affect the optical resonances of FP cavities. However, the vertical Brownian motion could make the stable suspension of nanoplates out of equilibrium. The normalized probability of the suspension distance due to the vertical Brownian effect is given by [53]:

$$\rho(d, T) = \frac{\text{Exp}[-U(d)/k_B T]}{\int_0^{\infty} \text{Exp}[-U(d)/k_B T] \partial d} \quad (6)$$

where  $U(d) = E_c(d) + F_{GB}d$  is the total energy of the suspended nanoplate, where  $F_{GB}$  is the sum of the gravity and buoyancy forces [41, 53]. Here, we consider the gold nanoplate with area  $A=20 \mu\text{m} \times 20 \mu\text{m}$  (see the experiment samples in [12]). The normalized probability with respect to the separation is shown in Figs. 5(a) and 5(b), where we set  $L_s=300$  and 150 nm, respectively. The higher of the probability at the equilibrium distance, the narrower the suspension distribution. The peak probability  $\rho(d_e, T)$  for  $L_s=150$  nm is almost 2 times larger than that of  $L_s=300$  nm, indicating a stronger stiffness at the

quantum trapping. Overall, the probability  $\rho(d_e, T)$  increases with increasing the applied voltage. By contrast, the probability  $\rho(d_e, T)$  decreases slightly with increasing the temperature from 300 to 350 and 400 K. The distribution functions could be overlapping with each other at an intervening 50 K. The average of separations would be [53]:

$$\bar{d} = \frac{\int_0^{\infty} d \cdot \text{Exp}[-U(d)/k_B T] \partial d}{\int_0^{\infty} \text{Exp}[-U(d)/k_B T] \partial d} \quad (7)$$

The  $\bar{d}$  is obtained by averaged over multiple measurements [12]. Here, the offset  $\Delta = \bar{d} - d_e$  given in Fig. 5 is smaller than 1 nm, due to the symmetry of the probability function near the equilibrium distance. The precise measurement of the thermal Casimir effect relies on the suspended separation of the nanoplate. Fortunately, the high  $Q$  spectra in optical cavities offer an opportunity to monitor the separation accurately. As depicted in the insets of Figs. 5(a) and 5(b), the high  $Q$ -factor is maintained over a wide range of separations. Compared with previous literature [50, 51], our work presents an accurate way to detect thermal Casimir effect via spectroscopic measurements of optical cavities.

#### IV. CONCLUSIONS

The optical FP cavities tuned by the Casimir forces is investigated in this work. The system consists of a gold nanoplate confronted to a Teflon-coated MOS substrate in a liquid environment. The suspension of the gold nanoplate is dependent on the balance among the Casimir, gravity and buoyancy forces. One way to modulate the suspension distance of the gold nanoplate is achieved by electrical gating. The frequency shifting of the reflection spectra can be tens of nanometers via gating voltages. Furthermore, the control of the optical resonances via the temperature is also demonstrated. The temperature modulations can be manifested greatly at sub-micrometer separations. In addition, the Brownian motion is discussed in different configurations. A new scheme to measure thermal Casimir effect is suggested by the spectroscopic measurements of the optical FP cavities.

#### Acknowledgments

This work is supported by the National Natural Science Foundation of China (Grant No. 11804288, and No. 61974127), Natural Science Foundation of Henan Province (Grant No. 232300420120), and the Innovation Scientists and Technicians Troop Construction Projects of Henan Province.

- 
- [1] H. B. G. Casimir, Proc. Kon. Ned. Akad. Wet. **51**, 793 (1948).
- [2] E. M. Lifshitz, Zhurnal Eksperimentalnoi Teoreticheskoi Fiziki **29**, 94 (1955).
- [3] L. M. Woods, D. A. R. Dalvit, A. Tkatchenko, P. Rodriguez-Lopez, A. W. Rodriguez, and R. Podgornik, Rev. Mod. Phys. **88**, 045003 (2016).
- [4] O. Kenneth, I. Klich, A. Mann, and M. Revzen, Phys. Rev. Lett. **89**, 033001 (2002).
- [5] R. Zhao, J. Zhou, T. Koschny, E. Economou, and C. Soukoulis, Phys. Rev. Lett. **103**, 103602 (2009).
- [6] M. Levin, A. P. McCauley, A. W. Rodriguez, M. T. H. Reid, and S. G. Johnson, Phys. Rev. Lett. **105**, 090403 (2010).
- [7] P. Rodriguez-Lopez and A. G. Grushin, Phys. Rev. Lett. **112**, 056804 (2014).
- [8] W. Nie, R. Zeng, Y. Lan, and S. Zhu, Phys. Rev. B **88**, 085421 (2013).
- [9] Z. Li and C. Khandekar, Phys. Rev. Appl. **16**, 044047 (2021).
- [10] M. Camacho, T. Gong, B. Spreng, I. Liberal, N. Engheta, and J. N. Munday, Phys. Rev. A **105**, L061501 (2022).
- [11] J. N. Munday, F. Capasso, and V. A. Parsegian, Nature **457**, 170 (2009).
- [12] R. Zhao, L. Li, S. Yang, W. Bao, Y. Xia, P. Ashby, Y. Wang, and X. Zhang, Science **364**, 984 (2019).
- [13] M. Dou, F. Lou, M. Boström, I. Brevik, and C. Persson, Phys. Rev. B **89**, 201407(R) (2014).
- [14] V. Esteso, S. Carretero-Palacios, and H. Míguez, J. Phys. Chem. C **119**, 5663 (2015).
- [15] X. Liu and Z. M. Zhang, Phys. Rev. Appl. **5**, 034004 (2016).
- [16] Y. Ye, Q. Hu, Q. Zhao, and Y. Meng, Phys. Rev. B **98**, 035410 (2018).
- [17] V. Esteso, S. Carretero-Palacios, and H. Míguez, J. Phys. Chem. Lett. **13**, 4513 (2022).
- [18] V. Esteso, S. Carretero-Palacios, and H. Míguez, J. Phys. Chem. Lett. **10**, 5856 (2019).
- [19] J. M. Vaughan, *The Fabry-Perot interferometer: history, theory, practice and applications* (Routledge, 2017).
- [20] V. Caligiuri, G. Biffi, M. Palei, B. Martín-García, R. D. Pothuraju, Y. Bretonnière, and R. Krahne, Adv. Opt. Mater. **8**, 1901215 (2020).
- [21] N. Liu, M. Mesch, T. Weiss, M. Hentschel, and H. Giessen, Nano Lett. **10**, 2342 (2010).
- [22] H. Deng, Z. Li, L. Stan, D. Rosenmann, D. Czuplewski, J. Gao, and X. Yang, Opt. Lett. **40**, 2592 (2015).
- [23] L. Ge, X. Shi, L. Liu, and K. Gong, Phys. Rev. B **102**, 075428 (2020).
- [24] T. Gong, B. Spreng, M. Camacho, I. Liberal, N. Engheta, and J. N. Munday, Phys. Rev. A **106**, 062824 (2022).
- [25] Q.-D. Jiang and F. Wilczek, Phys. Rev. B **99**, 125403 (2019).
- [26] R. Zeng and Y. Yang, Phys. Rev. A **83**, 012517 (2011).
- [27] J. Wang, X. Zhang, S.-Y. Pei, and D.-H. Liu, Phys. Rev. A **73**, 042103 (2006).
- [28] F. Chen, G. L. Klimchitskaya, V. M. Mostepanenko, and U. Mohideen, Phys. Rev. B **76**, 035338 (2007).
- [29] C.-C. Chang, A. A. Banishev, G. L. Klimchitskaya, V. M. Mostepanenko, and U. Mohideen, Phys. Rev. Lett. **107**, 090403 (2011).
- [30] V. A. Yampol'skii, S. Savel'ev, Z. A. Mayselis, S. S. Apostolov, and F. Nori, Phys. Rev. Lett. **101**, 096803 (2008).
- [31] E. G. Galkina, B. A. Ivanov, S. Savel'ev, V. A. Yampol'skii, and F. Nori, Phys. Rev. B **80**, 125119 (2009).
- [32] M. Boström, M. Dou, O. I. Malyi, P. Parashar, D. F. Parsons, I. Brevik, and C. Persson, Phys. Rev. B **97**, 125421 (2018).
- [33] L. Ge and X. Shi, Phys. Lett. A **450**, 128392 (2022).
- [34] M. Boström and B. E. Sernelius, Phys. Rev. Lett. **84**, 4757 (2000).
- [35] A. Sushkov, W. Kim, D. Dalvit, and S. Lamoreaux, Nat. Phys. **7**, 230 (2011).
- [36] M. Liu, Y. Zhang, G. L. Klimchitskaya, V. M. Mostepanenko, and U. Mohideen, Phys. Rev. B **104**, 085436 (2021).
- [37] C. Abbas, B. Guizal, and M. Antezza, Phys. Rev. Lett. **118**, 126101 (2017).
- [38] G. Bimonte, G. L. Klimchitskaya, and V. M. Mostepanenko, Phys. Rev. A **96**, 012517 (2017).
- [39] N. Khusnutdinov, R. Kashapov, and L. M. Woods, 2D Mater. **5**, 035032 (2018).
- [40] G. L. Klimchitskaya and V. M. Mostepanenko, Phys. Rev. B **91**, 174501 (2015).
- [41] L. Ge, X. Shi, Z. Xu, and K. Gong, Phys. Rev. B **101**, 104107 (2020).
- [42] M. Moazzami Gudarzi and S. H. Aboutalebi, Sci. Adv. **7**, eabg2272 (2021).
- [43] H. S. Sehmi, W. Langbein, and E. A. Muljarov, Phys. Rev. B **95**, 115444 (2017).
- [44] A. V. Krasavin and A. V. Zayats, Phys. Rev. Lett. **109**, 053901 (2012).
- [45] G. Jellison Jr and F. Modine, Appl. Phys. Lett. **69**, 371 (1996).
- [46] A. A. Banishev, C.-C. Chang, R. Castillo-Garza, G. L. Klimchitskaya, V. M. Mostepanenko, and U. Mohideen, Phys. Rev. B **85**, 045436 (2012).
- [47] F. Yi, E. Shim, A. Y. Zhu, H. Zhu, J. C. Reed, and E. Cubukcu, Appl. Phys. Lett. **102**, 221102 (2013).
- [48] G. T. Papadakis and H. A. Atwater, Phys. Rev. B **92**, 184101 (2015).
- [49] C. Sire, S. Blonkowski, M. J. Gordon, and T. Baron, Appl. Phys. Lett. **91**, 242905 (2007).
- [50] V. Esteso, S. Carretero-Palacios, and H. Míguez, J. Appl. Phys. **119**, 144301 (2016).
- [51] A. W. Rodriguez, D. Woolf, A. P. McCauley, F. Capasso, J. D. Joannopoulos, and S. G. Johnson, Phys. Rev. Lett. **105**, 060401 (2010).
- [52] T. Zhan, X. Shi, Y. Dai, X. Liu, and J. Zi, J. Phys.: Condens. Matter **25**, 215301 (2013).
- [53] J. Varela, A. W. Rodriguez, A. P. McCauley, and S. G. Johnson, Phys. Rev. A **83**, 042516 (2011).